ORIGINAL PAPER

Very Slow Creep Tests on Salt Samples

Pierre Bérest[1] · Hakim Gharbi[1] · Benoit Brouard[2] · Dieter Brückner[3] · Kerry DeVries[4] · Grégoire Hévin[5] · Gerd Hofer[6] · Christopher Spiers[7] · Janos Urai[8]

Abstract

The objective of this paper is to assess the creep law of natural salt in a small deviatoric stress range. In this range, creep is suspected to be much faster than what is predicted by most constitutive laws used in the cavern and mining industries. Five 2-year, multistage creep tests were performed with creep-testing devices set in a gallery of the Altaussee mine in Austria to take advantage of the very stable temperature and humidity conditions in this salt mine. Each stage was 8-month long. Dead loads were applied, and vertical displacements were measured through gages that had a resolution of 12.5 nm. Loading steps were 0.2, 0.4, and 0.6 MPa, which are much smaller than the loads that are usually applied during creep tests (5–20 MPa). Five salt samples were used: two samples were cored from the Avery Island salt mine in Louisiana, United States; two samples were cored from the Gorleben salt mine in Germany; and one sample was cored from a deep borehole at Hauterives in Drôme, France. During these tests, transient creep is relatively long (6–10 months). Measured steady-state strain rates ($\dot{\varepsilon} = 10^{-13}–10^{-12}$ s^{-1}) are much faster (by 7–8 orders of magnitude) than those extrapolated from relatively high-stress tests ($\sigma = 5–20$ MPa). When compared to $n = 5$ within the high-stress domain for Gorleben and Avery Island salts, a power-law stress exponent within the low-stress domain appears to be close to $n = 1$. These results suggest that the pressure solution may be the dominant deformation mechanism in the steady-state regime reached by the tested samples and will have important consequences for the computation of caverns or mines behavior. This project was funded by the Solution-Mining Research Institute.

List of Symbols

A, A_0, A_1, A_2	Constants of the constitutive law
c	Constant of the transient constitutive law
E	Elastic modulus
d	Cylindrical sample diameter
D	Grain diameter
h	Cylindrical sample height
K_0	Constant of the transient constitutive law
k_{salt}	Salt thermal diffusivity
K_{salt}	Salt thermal conductivity
m	Constant of the transient constitutive law
n	Exponent of the power law
P_{atm}	Atmospheric pressure
q	Constant of the hygrometry-sensitive constitutive law
t	Time
u_1, u_2, u_3, u_4	Relative displacements of the upper and lower platens
w	Constant of the hygrometry-sensitive constitutive law
Q_1, Q_2	Activation energy
R	Universal gas constant
T	Absolute temperature
α_{th}	Thermal expansion coefficient of salt
α	Rotation angle of the upper plate
β	Rotation angle of the upper plate
ε	Strain

✉ Pierre Bérest
berest@lms.polytechnique.fr

1 École Polytechnique, route de Saclay, 91128 Palaiseau, France

2 Brouard Consulting, Paris, France

3 Institut für Gebirgsmechanik, Leipzig, Germany

4 RESPEC, Rapid City, SD, USA

5 Storengy, Bois Colombes, France

6 Salinen Austria AG, Ebensee, Austria

7 Utrecht University, Utrecht, The Netherlands

8 Aachen University, Aachen, Germany

ε_{el}	Elastic strain
ε_{vp}	Viscoplastic strain
$\dot{\varepsilon}$	Strain rate
$\dot{\varepsilon}_s$	Steady-state strain rate
$\dot{\varepsilon}_t$	Transient strain rate
ε_t^*	Cumulated transient strain
η	Viscosity
θ	Characteristic transient time
σ	Deviatoric stress
σ_v	Stress level
Φ	Hygrometry

1 Introduction

Mines, brine production caverns, hydrocarbon storage caverns, and nuclear waste disposals have been implemented in salt formations. In such a context, a good understanding of the mechanical behavior of salt is required. Abundant literature has been dedicated to the various aspects of the creep behavior of salt (e.g., the proceedings of the nine conferences on the mechanical behavior of salt). During most of the laboratory tests, the applied deviatoric stress is in the 5–20 MPa range. However, Lux and Düsterloh (2015) note that:

.. . the stress levels in the large rock mass surrounding the cavity are well below the stress levels used in laboratory investigations. .. This means creep behavior for stresses levels $\sigma_v < 8$ MPa is not well based on observation in lab but based just on extrapolation.

Marketos et al. (2016) mention that:

Laboratory data on the low stress (hence low strain rate) steady state creep behavior of rock salt, however, are scarce as they are very difficult to obtain. .. a frequently-employed solution has been to extrapolate low stress behavior from higher stress or higher temperature tests, i.e., to use the same rock salt constitutive law for both high and low deviatoric stresses and strain rates.

However, such an extrapolation is not substantiated by analyzing deformation maps. Strong evidence shows that extrapolation dramatically underestimates the actual creep rate of rock salt at low stresses and has important consequences for the numerical computation of geological phenomena and long-term behavior of salt caverns or radioactive waste disposal. Van Sambeek and DiRienzo (2016) computed the closure rate of a borehole using a "segmented" creep law and stated that:

.. . even with small deviatoric stresses, the creep strain rates are larger than those predicted by most creep

laws. Because of this discrepancy, too-small structural responses are calculated as a consequence of using creep laws that under-predict creep rates for small deviatoric stresses.

Similar comments were made by Bérest et al. (2009) and Cornet et al. (2017).

Tests that were performed over the range of deviatoric stresses that coincide with field conditions are scarce, because strain rates during these tests are exceedingly slow at $\dot{\varepsilon} = 10^{-12}$ s^{-1} (3×10^{-5} per year). Daily room temperature fluctuations generate thermoelastic strains that are much larger than the strains to be measured. This problem can be solved by setting testing devices in an environment (e.g., a dead-end mine drift) that has exceedingly small temperature and humidity fluctuations (Bérest et al. 2005).

This paper is dedicated to 2-year, multistage, uniaxial creep tests that were performed in a mine drift of the Altaussee mine in Austria on salt samples that were cored from the Avery Island mine in Louisiana, United States; the Gorleben Mine in Germany; and a borehole drilled at Hauterives in France. The applied stresses were in the 0.2–1.0 MPa range, and five tests were performed in the frame of a collaborative research program that was funded by the Solution-Mining Research Institute (SMRI) (Bérest et al. 2017).

2 Salt Creep at High Stress

In this section, the main features of salt creep behavior at stresses greater than 5 MPa are described.

According to Bérest (2013) and other literature, the axial strain (ε), which is observed during a creep test that is performed on a cylindrical-shaped salt specimen in the laboratory, is the sum of three components: the thermoelastic strain (ε_{el}), the transient viscoplastic strain (ε_t), and the steady-state viscoplastic strain (ε_s). This is shown in Fig. 1 and mathematically expressed in one-dimensional (1D) rate form as

$$\dot{\varepsilon} = \frac{\dot{\sigma}}{E} - \alpha_{th}\dot{T} + \dot{\varepsilon}_s + \dot{\varepsilon}_t, \tag{1}$$

where contractive strains and compressive stresses are positive, σ is the applied stress during a uniaxial test, E is Young's modulus, T is the absolute temperature, and α_{th} is the thermal expansion coefficient of salt.

2.1 Steady-State Behavior

The steady-state viscoplastic component contribution to the total deformation is typically defined as a constant strain rate, $\dot{\varepsilon}_s$, that is reached after several weeks or months when the temperature, humidity, and deviatoric stress are
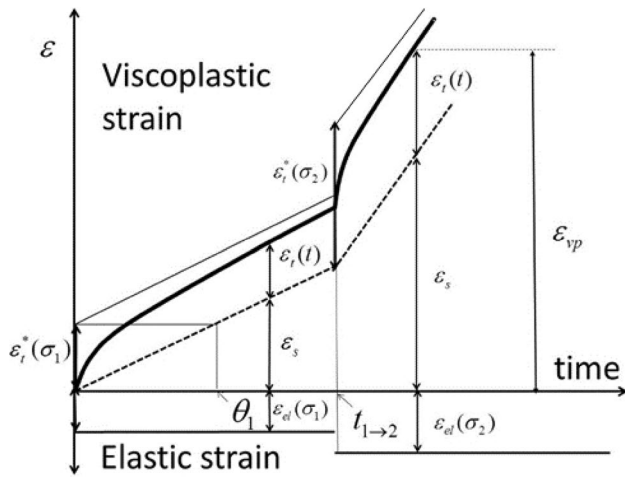
Fig. 1 Schematic strain–stress curve during an isothermal uniaxial creep test. At $t_{1 \to 2}$, the applied stress is increased from σ_1 to σ_2

kept constant. A simple formulation (Norton–Hoff's law, or "power" law) for a steady-state creep law is

$$\dot{\varepsilon}_s = A(\Phi) \exp(-Q/RT) \left(\frac{\sigma}{\sigma_0} \right)^n, \qquad (2)$$

where σ is the applied stress during a uniaxial test (or, more generally, $\sigma = \sqrt{3 J_2}$, where $J_2 = s_{ij} s_{ji}/2$ is the second invariant of the deviatoric stress tensor, $s_{ij} = \sigma_{ij} - \sigma_{kk} \delta_{ij}/3$); σ_0 is a reference stress, $\sigma_0 = 1$ MPa ; Q/R and n are two constants with n in the 3–6 range, the thermal constant (Q/R) is in the 3000–10,000 K domain, and $A = A(\Phi)$ is a function of the relative humidity (in %RH).

At a deviatoric stress of $\sigma = 10$ MPa and at ambient temperature, the steady-state strain rate for salt is typically of order of magnitude $\dot{\varepsilon}_s = 10^{-10}$ s^{-1}. For instance, Avery Island salt has been studied extensively at the RESPEC facility in Rapid City, South Dakota. The results of 55 of their creep tests are represented in a log $|\sigma|$-versus-log $|\dot{\varepsilon}_s|$ plot in Fig. 2. Note that the results of the low-stress tests performed at Varangéville (see Sect. 6.5.3) were also added. In principle, the mean stress has no influence on the steady-state strain rate, and no volumetric change is observed for typical confining pressures that are used for most triaxial creep tests. In fact, when loading is rapid, dilation (or even failure) is often exhibited under low or moderate confining pressures and high shear stresses (or tensile stresses), typically: $\sqrt{J_2} < f|I_1|$, where $I_1 = \sigma_{ii}$ is the first invariant of the stress tensor and f a constant, Van Sambeek et al. (1993): sample volume increases and the notion of a steady-state behavior does not apply anymore. In some cases, dilation does not appear immediately and failure is delayed. These issues have been discussed by many authors, for instance, Spiers et al. (1990), Thorel and Ghoreychi (1993), Chan et al. (1996), Cristescu and Hunsche (1998), Peach et al. (2001), Popp et al. (2002, 2012), and Schultze (2007). A formulation such that Eq. (2) holds only when the state of stress is such that salt behavior is not dilatant. In this paper, the applied stresses are small, strain rates are exceedingly slow, test duration is less than 2 years, and the cumulated strain at the end of a creep test is smaller than 10^{-3}. In such a context, dilation or failure is not expected to play a major role.

Fig. 2 Steady-state strain rate as a function of deviatoric stress and temperature for Avery Island salt (after DeVries 1988)
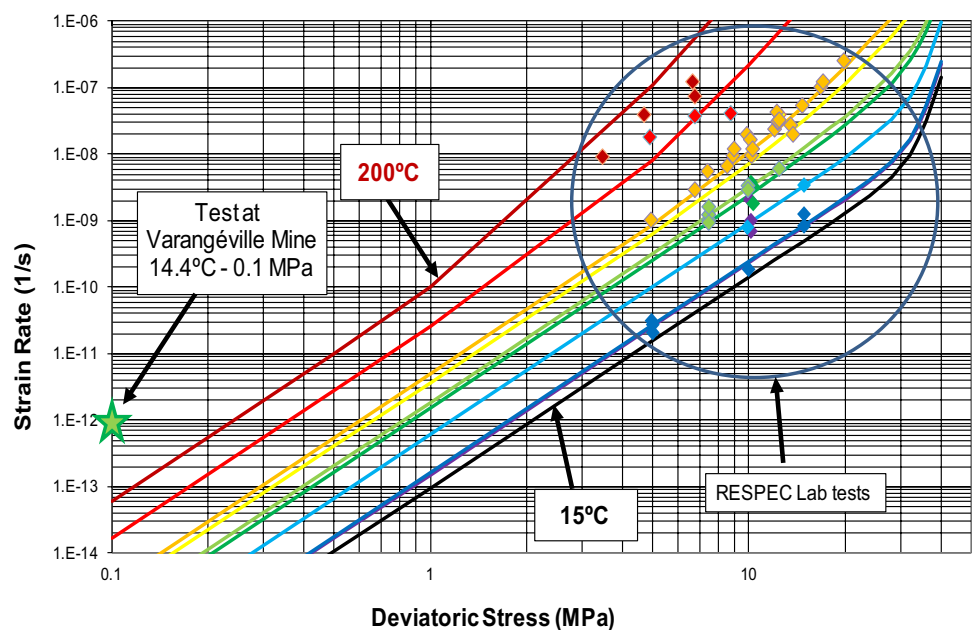
2.2 Transient Behavior

The transient component describes the rock's viscoplastic behavior before the steady state is reached. Any change in applied loading or temperature triggers a transient creep response. After a compressive load increase (i.e., direct creep), transient creep is characterized by faster initial strain rates compared to the steady-state strain rates. If the applied stress is kept constant after the stress changes, the transient rate slowly decreases until the transient strain exhausts itself, which is shown in Fig. 1. In other words, the total strain rate becomes equal to the steady-state rate and the transient strain reaches an asymptotic value that is defined as the transient strain limit $\varepsilon_t^* = \varepsilon_t^*(\sigma, T)$, which is a function of deviatoric stress and temperature. Munson and Dawson (1984) suggested:

$$\varepsilon_t^* = K_0 e^{cT} \left(\frac{\sigma}{\sigma_0} \right)^m, \tag{3}$$

where K_0, c, and m are three material constants ($m = 3$ is typical); $\sigma_0 = 1$ MPa.

A characteristic time, $\theta(\sigma, T)$ (Fig. 1), can be defined as the time after which, given σ and T, the accumulated steady-state strain $(\dot{\varepsilon}_s \theta)$ is larger than the asymptotic transient strain (ε_t^*):

$$\theta(\sigma, T) = \varepsilon_t^* / \dot{\varepsilon}_s = K_0 e^{cT + Q/RT} \left(\frac{\sigma}{\sigma_0} \right)^{m-n} \Big/ A. \tag{4}$$

This time provides a measure of the duration of the transient phase. Djizanne Djakeun (2014) estimated values of θ ranging between 0.5 and 5 years for 12 different salt formations at $\sigma = 10$ MPa and $T = 310$ K. In principle, θ is a decreasing function of the applied stress, because n is typically greater than m.

Although other formulations can be selected, Norton–Hoff and Munson's constitutive laws capture the main features of transient and steady-state creep behavior under high stress and will be used for interpreting, at least in a qualitative way, the main results of the creep tests that are performed under low stresses.

2.3 Hygrometry

Hygrometric variations can also be a concern at a laboratory scale (Horseman 1988; Hunsche and Schulze 1996, 2002) and in room-and-pillar mines (Van Sambeek 2012). Hunsche and Schulze (1996) suggested that when hygrometry is taken into account, the steady-state creep rate must be corrected as follows:

$$\dot{\varepsilon}_s = A_0(T) \big[1 + w \sinh(q\Phi) \big] \exp(-Q/RT) \sigma^n, \tag{5}$$

where $0 < \Phi < 100$ is the relative hygrometry (%RH) in the testing room given as a percentage.

The two constants (q and w) have values of 0.1. A change in the room hygrometry from $\Phi = 55\%$RH to $\Phi = 75\%$RH leads to a factor of 7 increase in the steady-state rate. Humidity is especially effective when the air can enter the sample [e.g., after onset of dilation and after the sample begins micro-fracturing (Hunsche and Schulze 2002)]. The effect of humidity is likely related to water sorption onto cracked surfaces and grain boundaries, which accordingly influence dissolution/precipitation and diffusive transport processes (Koelemeijer et al. 2012).

2.4 Extrapolation to Low Stresses

Langer (1984) stated that reliably extrapolating the creep equations at low deformation rates can only be carried out on the basis of deformation mechanisms. The micro-mechanisms that govern salt creep have been discussed by Munson and Dawson (1984), Langer (1984), Blum and Fleischman (1988), and Hampel (2015). A deformation-mechanism map that was adapted from Munson (1979) is presented in Fig. 3.

The upper shaded rectangle in Fig. 3 is the domain inside which most laboratory tests are performed, the larger rectangular domain is the domain of interest for designing caverns and mines, and the approximate testing conditions during the Altaussee tests are indicated by a star. Not only are data limited in the low-stress domain (< 5 MPa), but the micro-mechanisms that govern creep in this domain are not fully understood. Predicting the mechanical behavior of salt in this domain is based on extrapolating purely empirical data,
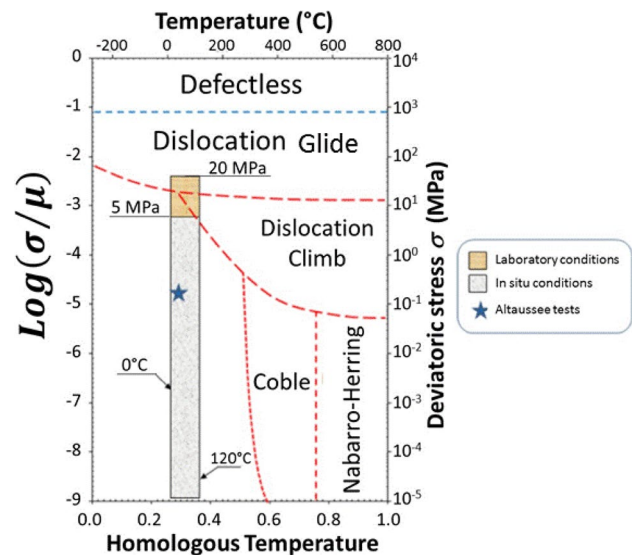

Fig. 3 Deformation-mechanism map (Adapted from Munson 1979); μ is the elastic shear modulus. The blue star represents the testing conditions during the Altaussee tests

an extrapolation that cannot be supported by theoretical consideration.

However, Spiers et al. (1990) and Urai and Spiers (2007) observed that pressure-solution creep, which is an important deformation mechanism of most rocks in the Earth's crust, is especially rapid for rock salt in the low-stress domain. Theoretical findings and experimental evidence strongly suggest that the relationship between deviatoric stress and strain rate is linear for this mechanism. According to the literature (Peach et al. 2001; Ter Heege et al. 2005a, b; Urai and Spiers 2007; Urai et al. 2008), modestly accelerated dislocation creep behavior in the transitional region between dislocation-dominated flow and pressure-solution creep is caused by rapid, dynamic recrystallization that involves fluid-assisted grain-boundary migration. In this context, water content in the sample and grain size play a significant role during a creep test.

Possible field evidence that indicates a transition from power law, dislocation creep at high stresses to linear, and pressure-solution creep at low stresses was discussed by Campos de Orellana (1996), Breunesse et al. (2003), Urai and Spiers (2007), and Cornet et al. (2017). Brouard et al. (2013) measured a volume-loss rate of a brine-filled cavern at a depth of 250 m that was slightly less than 10^{-5}/year $\approx 3 \times 10^{-13}$/s, which is a small value but faster than what can be extrapolated from nearly all salt creep models. This transitional behavior is considered in a few models [e.g., Lubby2 (Rokahr et al. 2011) and CDM (Hampel 2015)]. Marketos et al. (2016) also used a combined linear (i.e., pressure-solution creep) and power-law (i.e., dislocation creep) model to assess the subsidence above hydrocarbon storage caverns with overlying evaporate rocks. The functional form of the model used by Marketos et al. (2016) is given by

$$\dot{\varepsilon}_s = A_1 \exp\left(-Q_1/RT\right)\left(\frac{\sigma}{\sigma_0}\right)^n + \frac{A_2}{D^3}\exp\left(-Q_2/RT\right)\frac{\sigma}{\sigma_0}, \tag{6}$$

where D is the grain size and the other parameters are the same as discussed above. When the applied stress is low, the power-law term is negligible, and the opposite is true when the applied stress is high. How other features of high-stress creep behavior (e.g., influence of humidity, dilatation, dislocation creep, and transient creep) are modified in the low-stress domain is still largely unknown.

3 Temperature, Humidity, and Atmospheric Pressure During the Creep Tests

3.1 A Comment on Temperature Effects During a Creep Test

When performing low-stress creep tests, temperature fluctuations are greatly concerning. These fluctuations generate additional thermoelastic strain, $\Delta\varepsilon = -\alpha_{th}\Delta T$ (i.e., contractive strains are positive), and modify the transient and steady-state viscoplastic strain rates. Using the Norton–Hoff relationship given in Eq. 2 $\left(\Delta\dot{\varepsilon}_s/\dot{\varepsilon}_s = Q\Delta T/RT^2\right)$ and assuming $Q/R = 4000$ K and $T = 280$ K, the relative change for the steady-state strain rate for a temperature change of 0.1 °C is quite small (0.005). The same cannot be said of thermoelastic strains. Consider a test, where the applied stress is controlled perfectly. When steady state is reached, Eq. (1) becomes

$$\dot{\varepsilon} = \dot{\varepsilon}_{vp} - \alpha_{th}\dot{T}. \tag{7}$$

When the creep rate is $\dot{\varepsilon}_{vp} = 10^{-12}$ s^{-1}, a test that lasts 36 days (3×10^6 s) results in an accumulated viscoplastic strain of $\Delta\varepsilon_{vp} = 3 \times 10^{-6}$. The thermal expansion coefficient of salt is approximately $\alpha_{th} = 4 \times 10^{-5}$ /°C. If the room temperature at the end of the test is warmer than at the beginning of the test by $\Delta T = 0.1$ °C, then the thermal strain $\left(\alpha_{th}\Delta T = 4 \times 10^{-6}\right)$ is larger than the accumulated viscoplastic strain $\left(\Delta\varepsilon_{vp}\right)$.

In a standard laboratory-testing room, avoiding temperature fluctuations as small as 0.1 °C is practically impossible, and wrong conclusions may be drawn from the test results. This problem can be solved by two methods.

The first method consists of designing a special testing chamber in which temperature fluctuations are made quite small; such a device was built and operated by Hunsche (1988). In a test that used this device and lasted approximately 1 week, "the lowest reliably determined deformation rate" was $\dot{\varepsilon} = -7 \times 10^{-12}$ s^{-1} (Hunsche 1988). Temperature fluctuations measured during this test were less than 0.001 °C. The main drawback of this system is the cost of developing the environmentally controlled chamber.

The second method consists of setting the testing device in an environment with exceedingly small temperature fluctuations (e.g., a dead-end mine drift). In a mine environment, tests can be quite long and potentially last several years. The main drawback of this second approach is that the testing temperature (and hygrometry) cannot be varied. The testing devices shown in Fig. 4 were positioned at the midlength of a dead-end mine drift of the Altaussee salt mine in Austria and operated by Salinen in Austria, operated at a 150-m distance from the main gallery.

Fig. 4 Testing devices in a dead-end gallery at the Altaussee mine

3.2 Temperature and Humidity in the Mine Drift During the Testing Period

Three platinum temperature sensors were set in the mine drift 1 year before the creep tests began (December 2013). Their resolution is 0.001 °C. They proved that natural temperature fluctuations were small (a few hundreds of °C); they origin at least partly from the expansion–contraction of the air generated by atmospheric pressure fluctuations, whose effects, however, are considerably attenuated by heat exchange through the gallery walls, as was observed by Perrier et al. (2010).

With help from mine personnel in June 2014, the gallery was equipped with a door at the testing room entrance to minimize the air circulation and temperature fluctuations, which became ± 0.01 °C. As expected (Sect. 3.1), a clear correlation was observed between temperature fluctuations and measured strains. However, as heat transfer through conduction in the samples is relatively slow (1 h, i.e., the same order of magnitude that temperature fluctuations period), correction of strains for the effects of temperature was far from perfect. In addition to hourly fluctuations, a very slow temperature drift was observed. The gallery temperatures during each of the three stages of testing include the following:

- Stage 1 (August 2014–July 2015): slow temperature increase of 0.1 °C per year (°C/year)
- Stage 2 (August 2015–March 2016): slightly faster temperature decrease of -0.2 °C/year
- Stage 3 (April 2016–November 2016): minute temperature changes.

Section 2.3 mentioned that the effect of hygrometry on the sample strain rate is significant. Two humidity gages were set in the Mine 1 year before the test starts. They were calibrated using a high-accuracy gage. From August 2014 to November 2016, the humidity increased from 67.5 to 68%RH, a small difference. Based on the work of Hunsche

and Schultze (1996), a $\Delta\Phi = 0.5\%$ RH change in relative humidity generates a $\Delta\dot{\varepsilon}/\dot{\varepsilon} = 5\%$ strain-rate change, which is a small value of insignificant consequence.

More information on temperature and hygrometry can be found in the SMRI Report (Bérest et al. 2017).

4 Testing System

4.1 Testing Device

During a creep test, fluctuations in the applied stress (Wawersik and Preece 1984) are a concern, because they lead to changes in the transient strain (see Sect. 2.2). When the applied load is increased relatively quickly (e.g., 1 day) and then returned to its initial value, the strain rate does not return to the rate before the load change for several days or more, which is an effect of "reverse" creep (Bérest et al. 2015). During the Altaussee tests, dead weights were used to apply a constant load to the test specimens. Cylindrical salt samples ($d = 70$ mm, $h = 140$ mm; or $h = 120$ mm in the case of the Hauterives sample) were set between two horizontal duralumin plates, which are illustrated in Fig. 5. The lower duralumin plate is fixed to the testing frame. Dead weights are added to the lower part of a mobile rigid frame, which transmits the mobile frame weight to the upper duralumin plate through a small metallic ball. The applied stress is calculated by dividing the overall weight of the steel frame by the initial cross section of the salt cylinder. Note that no attempt was made to correct the applied stress for diameter changes, which are smaller than $\Delta d/d = 10^{-4}$ after a 2-year test for the small loads applied. The stresses that can be applied to a sample using the testing apparatus range are between 0.05 and 1 MPa.

4.2 Measurement of Axial Displacement

The objective of this paper is to discuss experimental results obtained in the small strain domain (smaller than 10^{-3}). For this reason, the computed axial strain is the "engineering" strain, or $(h - h_0)/h_0$ (contractions are negative) and the computed axial strain rate, or $\dot{h}/h_0$, (contraction rates are negative), is computed as follows.

The creep rate can be computed by comparing strains, $\varepsilon_1 = \delta h_1/h_0$ and $\varepsilon_2 = \delta h_2/h_0$, that are measured at two different times, t_1 and t_2, or $\dot{\varepsilon} = (\varepsilon_2 - \varepsilon_1)/(t_2 - t_1)$. For example, when $t_2 - t_1 = 10^5$ s (1 day) and $\dot{\varepsilon} = 10^{-12}$ s^{-1}, then $\varepsilon_2 - \varepsilon_1 = 10^{-7}$; a reasonable assessment of weekly strain-rate demands strain be measured with an accuracy of 10^{-7}, which is a displacement of approximately 10^{-8} m (0.01 μm). Special sensors (i.e., Solartron linear encoders) were used to measure the displacement. Sensor accuracy and resolution are 0.5 and 0.0125 μm (1/80 μm), respectively. Displacements are

Fig. 5 Testing device. **a** (Left). The picture displays the three-leg testing frame, the salt sample (upper part of the mobile frame), and the circular plate on which dead weights are applied (lower part of the mobile frame). **b** (Right) Adjusting the displacement gages around the salt sample

measured every 60 s. The encoders operate on the principle of interference between two diffraction gratings, which are deposited on a quartz substrate. The gratings are composed of black and white, 10-μm-long, rectangles. A first grating is illuminated by a light-emitting diode and a second grating is used to scan the modulated light intensity that is generated when the first grating moves because of sample deformation. The system computes displacements based on how many rectangular intervals cross a stationary reference. A drawback of this system is that the counting is reset to zero at any electric outage. Several electric outages occurred inadvertently because of staff member activity in the room. Fortunately, corresponding offsets could be reconstructed to provide continuous strain-versus-time curves throughout the duration of the tests.

4.3 Rotation of the Upper Plate

Because the lower duralumin plate is fixed, purely rigid movement (i.e., rotation + vertical displacement) of the stiff mobile upper plate can be expected. To detect such movements, three vertical displacement gages are needed. To provide some redundancy, four high-resolution displacement sensors are positioned in two vertical planes at a 90-degree angle.

Because test durations were approximately 2 years, sensor drift can lead to measured inaccuracy, which must not be confused with the actual creep of the sample. The absence or presence of sensor drift was confirmed by properly assessing the data. For example, the four displacement-versus-time curves (u_1, u_2, u_3 and u_4) do not overlap, which raises concerns about sensor accuracy; these displacements are shown

in Fig. 6. However, if the results of the two sensors along the same axis are averaged, $(u_2 + u_4)/2$ and $(u_1 + u_3)/2$, the two curves almost perfectly overlap, which proves that this plate has rotated, the four displacement measurements are consistent, and the sensors have drifted very little or not at all. An abrupt rotation of the upper plate was observed in September 2014 when a small piece of salt fell from the roof, landed on the upper plate, and caused abrupt differential displacement that was detected by individual sensors (see Fig. 6). However, the average displacement values remained consistent. In Fig. 6, the rotation of the platen is identified, wherein β is the angle between the vertical direction and the normal to the upper platen and α is the angle between a diameter of the platen (which is fixed with respect of the platen) and this diameter of the platen which is horizontal at a given instant. Both stabilize after several months, and a possible explanation for this occurrence is proposed in Sect. 6.2.

During each of the three testing stages, several sensors failed. The number of reliable sensors during each stage for each of the five samples is provided in Table 1. At the end of each stage, the out-of-order displacement sensors were replaced.

4.4 Computation of Strain Rates

During a creep test, the ability to compute strain rates is essential. However, strains experience fluctuations (e.g., because of temperature changes) that make rate computation difficult. During the tests, the average strain rate over a specified time interval was computed through the least-squares
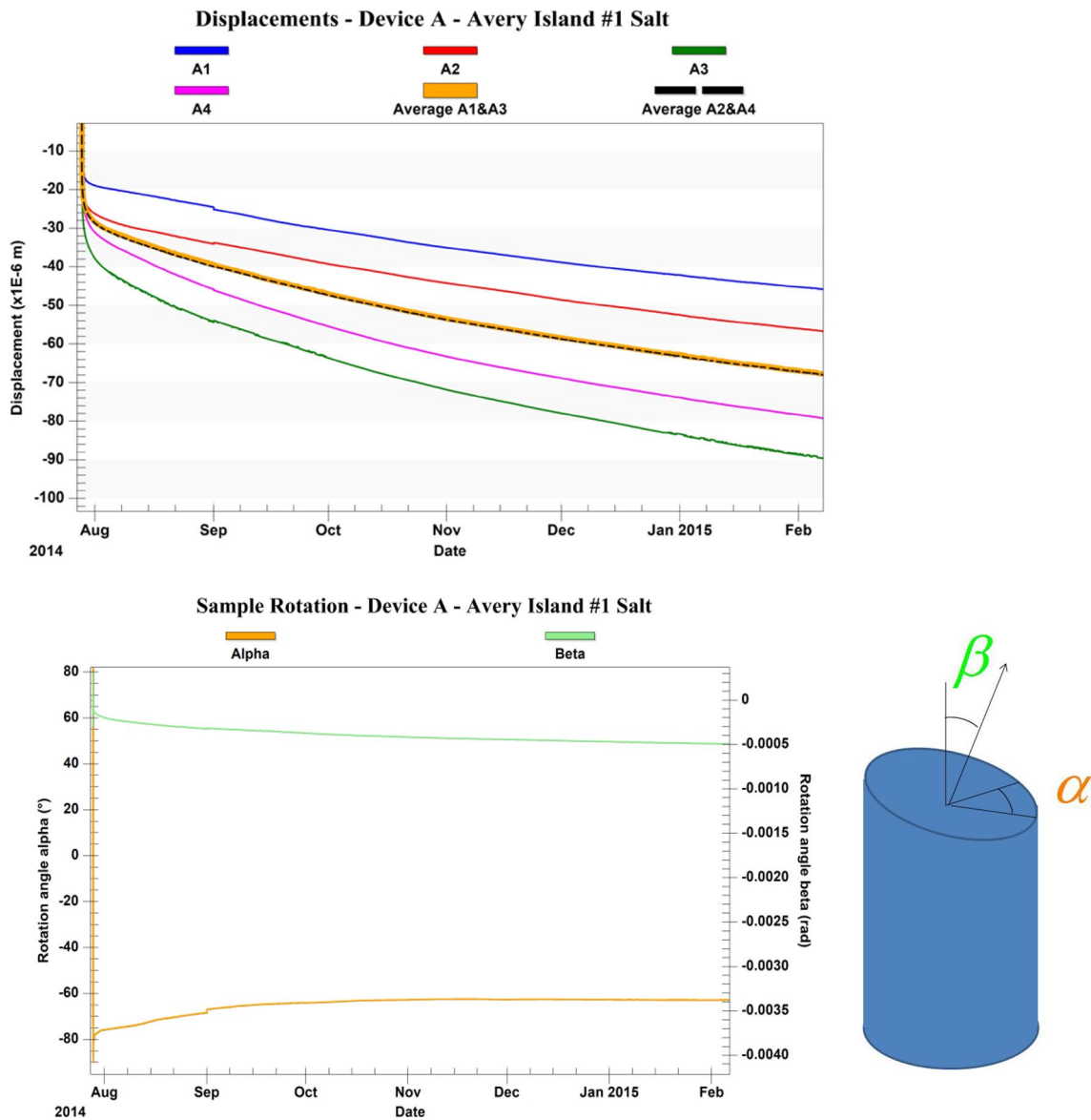
Fig. 6 Four vertical displacements and their average values during a creep test on an Avery Island salt sample (top) and platen rotation (bottom). The applied load is 0.2 MPa

Table 1 Number of sensors

Device (sample)	A (AI #1)	B (AI#2)	C (HR#1)	D (Go#1)	E (Go#2)
First stage	4	4	3	4	3
Second stage	3	2	3	4	4
Third stage	3	4	3	4	3

method. The computed strain rate is sensitive to the interval length, and a selected interval of 10 days was found to provide a representative response. 14,400 strain values, or

approximately 1 per minute, are taken into account to compute a strain rate.

During a creep test, the strain rate consistently decreases. Microstructural analyses strongly suggest that, after some time, the strain rate is constant and a steady state is reached. However, when analyzing the results of a creep test, no objective criterion shows that steady state is reached. In this paper, a constant load is applied over 8 months, and steady state is assumed to be reached when strain-rate variations remain consistently small during a sufficiently long period (e.g., 1 month). A 10-year test would likely lead to a different conclusion.
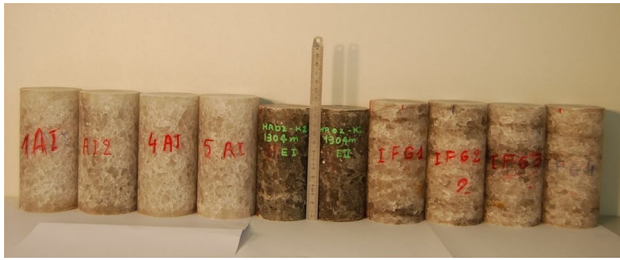
Fig. 7 Ten samples set in the gallery at the beginning of the test (IFG#1 sample is called Gorleben #1, or Go#1 in this paper)

5 Specimens

5.1 Salt Samples

Ten samples were available for creep testing and are shown in Fig. 7. Two samples from the Avery Island mine (AI #1 and #2), one sample from the Hauterives (HR #1) drillhole, and two samples from the Gorleben mine (Go #1 and #2, also called IFG #1 and #2) were tested. The Avery Island and Gorleben samples were 14 centimeters (cm) high, and the Hauterives sample is 12 cm high. Several cubes were cut from the same blocks that were used to core the samples (Sect. 5.2). The grain sizes of the selected samples were determined by applying the linear intercept method to the lines drawn on scans of the cylindrical sample surface, which yielded the values shown in Fig. 8. Table 2 shows the linear intercept data per sample investigated. Creep tests had been performed on AI #1 and Go #2, while AI #5, HR #2 and Go #3 had been kept in the gallery for more than 2 years with no load applied when grain sizes were determined.

The salt from the Avery Island mine comes from the diapirism of the underlying Luann Salt that formed during the Callovian in the mid-Jurassic and has been extensively studied. Petrography studies document that the Luann Salt is a relatively pure (typically 98% halite), homogeneous, domal halite with minor amounts of anhydrite and argillaceous (clay) at the grain boundaries (Carter and Hansen 1980). Crystal sizes range from 2.5 to 15 mm and average approximately 7.0–9.0 mm, as shown in Table 2. The core was taken from the floor of a room near the center of the dome at the
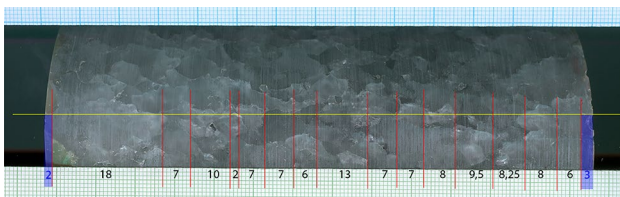

Fig. 8 Grain-size determinations for selected samples shown in Fig. 9. The photograph illustrates the linear intercept method as applied to a scan of Sample AI #5. Table 2 shows the linear intercept data per sample investigated

Table 2 Linear data intercept method

Length (mm)	AI #1 137.75	AI #5 134	Go #2 138.75	Go #3 139.5	HR # 2 128.25
Grains number	19	15	35	39	12
Mean	7.3	8.9	4.0	3.6	10.7
Standard dev.	3.2	5.8	2.1	1.8	6.5

150 m (500 ft) mining level in the early 1980s. The depth below the floor, where the specimens were obtained, was nominally 3.5 m (12 ft). The core was sealed with multiple layers of plastic wrap and wax, stored in an environmentally controlled location for preservation, and not exposed until a few months before testing.

The salt from the Gorleben Mine belongs to the Hauptsalz of the Staßfurt-series (z2HS), which forms the inner core of the Gorleben dome and contains 2–5% anhydrite. The mean grain size of the samples studied was approximately 3.5–4.0 mm, which is shown in Table 2. Diapirism homogenized the salt into a mixture in which (Hammer et al. 2015):

> … blocks of primary rock salt crystals, and shredded and crushed fragments of anhydrite lines, float in a matrix of recrystallized rock salt … Original brine trapped in the salt was … squeezed up to the salt table … dissolution films on grain boundaries ... form isolated fluid inclusions.

The Gorleben salt contains locally varying amounts of hydrocarbons from its sedimentary or tectonic history, which is seen in many domal salt structures. Hammer et al. (2015) have stated that:

> Hydrocarbons appear mostly in the form of streaks, dispersed clouds, clusters and islands ... hydrocarbons are located (1) along grain boundaries of halite and/or anhydrite crystals (2) in newly formed artificial microcracks due to drilling and preparation (3) in μ-capillary tubes of anhydrite crystals and (4) rarely in μ-porous parts of the Hauptsalz … the content (up to several hundred ppm) is too low to affect the geomechanical behavior of rock salt.

The Hauterives salt, which formed during the Sannoisian (Oligocen), belongs to the Valence subsidence basin. Samples were cored from the HR02 well at a 1304-m depth. The sample content was 65% halite and enriched by more or less diffuse anhydrite (30%) and marls (5%). The mean grain size of the investigated sample was approximately 10–11 mm (Table 2).

5.2 Water Content

Because pressure solution was suspected to play a significant role at low stress, water content was measured at Utrecht University (Table 3) on 50-mm salt cubes that were cored from the Avery Island, Hauterives, and Gorleben salt blocks that had been used to prepare the test samples. A state-of-the-art Fourier Transform Infrared (FTIR) Spectrometer (Jasco Instruments) was used to send a wide infrared (IR) beam (approximately 5-mm diameter) through the central region of each sample (50 mm × 50 mm × 50 mm), which makes IR absorption measurements in three directions at right angles. NaCl is completely transparent to IR radiation, so the FTIR technique is very suitable for measuring the water content of salt. Measurements were made along a 20-mm-long path through polished windows that were machined into the sample by dry drilling/polishing. The total water present in the form of liquid brine was measured by integrating the area under the absorption peaks that corresponds to the H_2O-stretching vibration in the saturated brine. These measurements are unaffected by any present hydrocarbons, which generate easily distinguishable spectra.

The results of using this approach are in parts per million (ppm) by mass. The effects of atmospheric water content, other phases, and impurities on the signal are removed by subtracting the background-transmitted IR intensity; therefore, the results reflect the true liquid–water content that is present only in the brine. This brine is present in fluid inclusions and films within the grain boundaries [where they potentially promote deformation processes (e.g., fluid-assisted recrystallization and pressure solution)] and in fluid inclusions that are trapped within individual salt grains.

Some variability in the measurements can be expected, because the sample size is relatively small in relation with the grain size. Because the approach to determine the water content of the samples depends in part on the number, size, and orientations of grain boundaries within the region analyzed, the specific location within the block from which the sample was taken affects the results. In addition to grain-scale variability, water content will also vary at large scales, which were impossible to quantify given the limited salt core available.

The measured values still fall within the ranges that were expected and previously measured for natural salt (approximately 50–5000 ppm) and confirm what was measured at Texas A&M University on the Avery Island salt (< 100 ppm), which is a very dry salt (Carter et al. 1993). The Gorleben sample (500 ppm = 0.05 wt%) has a slightly higher water content than the average value for the Gorleben salt measured by Bornemann et al. (2008) (0.012–0.017 wt%). These water quantities are expected to affect the mechanical behavior of salt if the water does not escape because of dilatancy and/or drying. Water content as low as 10 ppm can significantly affect the mechanical behavior compared with dried material that contains less than 5 ppm (Ter Heege et al. 2005a).

6 Test Results

6.1 Applied Loads

With support from the Salinen Austria personnel, the testing apparatuses and salt specimens (with no load applied) were set in a semicircular arrangement in the gallery in early July 2014 with three temperature sensors and two humidity sensors positioned at the center of the half-circle. The objective was for the specimens and drift to reach thermal equilibrium before initiating the tests. Before beginning the tests in August 2014, a neoprene jacket was set around one of the Avery Island samples (AI #1), and the jacketed sample was set in an oil-filled cylindrical container to protect the sample from the effects of humidity changes. The other specimens were not jacketed and were exposed to humidity changes. Directly comparing the results of AI #1 with the responses of the other specimens allows the effect of humidity changes to be quantified.

The literature contains many references to testing procedures, where an isotropic compressive stress is applied to the sample before testing in an effort to heal the damage created by stress relief during coring and sample preparation. In some cases, the compressive stress is retained (not unloaded) before testing of the sample is initiated. No effort was made to precondition the samples before testing while completely removing a relatively large isotropic preconditioning compressive stress, believed to be necessary to heal the specimen in a short period of time, would create new damage to the samples. This choice is arguable but later substantiated after a 5 MPa confining pressure was applied to one of the Avery Island samples (Sect. 6.5).

On August 1, 2014, a 0.2-MPa load was applied to each sample (Table 4). At the planned end of the first stage (8 months later), only the Hauterives sample appeared to have reached steady state. Therefore, the tests were continued without increase in loading for an additional 3 months. Because of an electric power outage, no data were collected between April 2015 and June 2015; however, the specimens are believed to have continued to deform as expected during this period.

The second stage of each test officially began on July 6, 2015, 11 months after the initial loading. Loads were increased to 0.4 MPa on the AI #1, HR #1, and Go #2 samples. Because the strain rates of AI #2 and Go #1 were still

decreasing noticeably, the load was not increased during the second stage for these two tests; the load was maintained at the same level as that of the first stage (0.2 MPa). The loads during the second stage were held constant without incident for approximately 9 months.

The third stage began on April 6, 2016, and ended approximately 8 months later in December 2016. Loads during the third stage were increased to 0.6 MPa, as initially planned, except for the Go #2 sample. The load on this sample was increased to 1.07 MPa to test the limits of the loading system.

The evaluation of the provided results focuses on four specific topics: (1) the duration of the transient creep phase; (2) the effect of hydrocarbons in the Gorleben salt; (3) the Hauterives salt's unique behavior; and (4) the strain rates measured during the tests.

6.2 Transient Strain Rate

Transient creep responses were evident in the measured responses for all of the samples immediately after each load change. The transient creep response lasted more than 8 months for all of the samples, except the Hauterives salt sample. As mentioned in Sect. 4.4, defining the end of the transient phase for a creep test is difficult regardless of the magnitude of the applied stress or temperature. The plot of strain rate-versus-time of AI #2 (shown in Fig. 9) demonstrates a prime example of this difficulty. The sample was subjected to a 0.2 MPa load for 20 months with steady state likely reached by the end of the test. The strain rate is clearly decreasing during the first 8 months and continues to decrease slightly after resuming data collection in July 2015 at 11 months. However, the precise ending of the transient phase cannot be discerned from Fig. 9. Transient phase durations that are greater than 8 months may seem

surprisingly long, because most creep tests documented in the literature are completed in a fraction of the time. Because many of the creep tests documented in the literature only present measured outputs for strain and time and do not allow for accurately accessing the end of the transient phase, the steady state may not be reached by a significant number of short-term tests. However, steady state is likely achieved much more quickly for tests that are conducted at higher strain rates, see Sect. 2.2.

As exhibited by Eq. (3), a factor of 2 increase in the applied stress should result in an increase for the accumulated transient strain, ε_t^*, by a factor of 8. When the stresses were increased from 0.2 to 0.4 MPa between the first and second stages, the transient strain observed for each of the tests was assumed to be nearly 8 times greater; however,

Table 3 Water content in selected salt samples

	Path length (mm)	Peak area (mm^2)	Parts per million H$_2$O	Axis
Reference	50	22.6	42	
Go cube	20.4	127	578	x
	19.8	49.7	233	y
	20.05		626	z
Mean			479	
AI cube	20.7	9.6	43	x
	19.8	18.3	86	y
		12.1	66	z
Mean			65	
	21.3	25	109	x
	21.9	15.9	67	z
HR cube	22.1	nm	nm	y
	17	nm	nm	y
	12	nm	nm	y
Mean			88	

nm nothing measured; insufficient transparency to obtain signal

Fig. 9 Computed strain rate as a function of time, AI #2 salt sample

Table 4 Loads applied on the samples

Device (sample)	A (AI #1) (MPa)	B (AI #2) (MPa)	C (HR #1) (MPa)	D (Go #1) (MPa)	E (Go #2) (MPa)
First stage 8-1-2014–7-5-2015	0.2	0.2	0.2	0.2	0.2
Second stage 7-6-2015–4-5-2016	0.4	0.2	0.4	0.2	0.4
Third stage 4-6-2015–12-2016	0.6	0.6	0.6	1.07	0.6

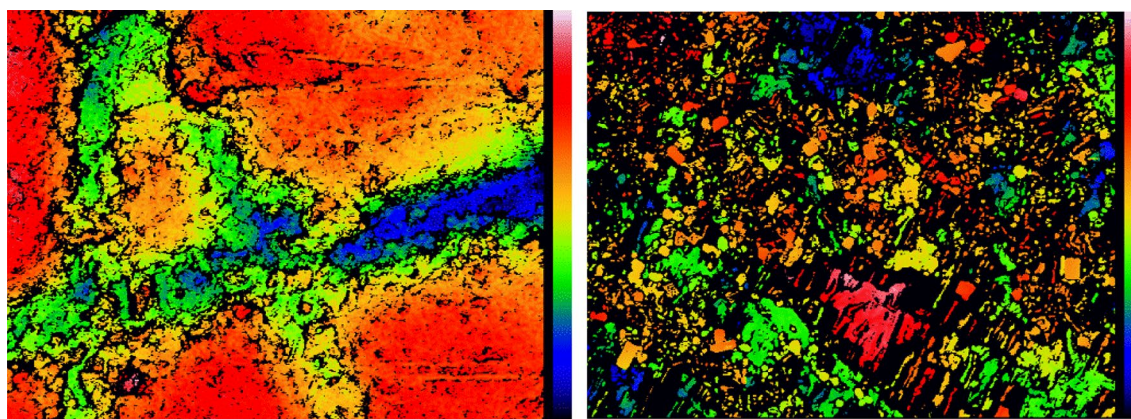**Fig. 10** Irregularities on the faces of two salt specimens that vary by 15 μm (left) and 29 μm (right). The microphotography picture size is 0.3 mm×0.22 mm (640×480 pixels)

this was not the case. Several reasons can be suggested to explain this finding and several other explanations may exist. Munson's model for transient creep could be irrelevant when small stresses are considered, or larger apparent transient effects could be caused by vertical irregularities that result from sample preparation on the lower and upper faces. Asperities were measured on two samples at a height or depth of ± 8 and ± 15 μm, respectively, which is shown in Fig. 10. When a vertical load is applied for the first time, these irregularities are flattened or crushed, because they

are submitted to high stresses that result in much faster creep and a possible rotation of the upper plate (Sect. 4.3). Strains generated by such effects are of order of magnitude $10\,\mu m/10\,cm = 10^{-4}$. Such deformation or crushing may be much less effective for subsequent load applications, even if the subsequent loads are relatively larger.
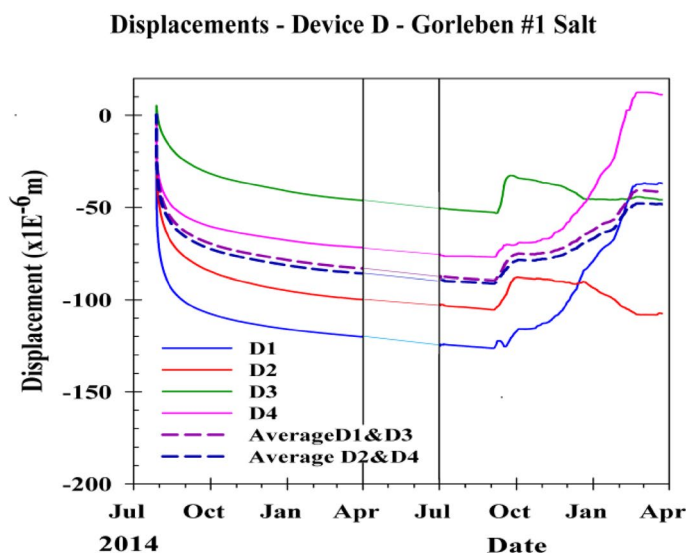

Fig. 11 Hydrocarbons at the bottom of the Go #1 sample device *D* (left), and displacements during Stages 1 and 2 (right). The four vertical displacements (*D*1 − *D*4) are shown together with the averages

(*D*1 + *D*3)/2 and (*D*2 + *D*4)/2. Swelling and upper plate rotation can be observed in September 2015

6.3 Problems Raised by Hydrocarbons Contained in Gorleben Salt

Section 5.1 mentioned that the Gorleben salt sometimes contains hydrocarbons and small amounts of anhydrite (up to 10%). During the first creep stage, liquid hydrocarbons were found at the bottom of the Go #1 and Go #2 samples (Fig. 11). The hydrocarbons were hypothesized to have not been squeezed out by the stress applied to the sample (this stress is quite small) but expelled by the combined difference in surface tension between oil and salt and brine and salt. The uptake of water by hydration from the mine air that was needed to produce this effect might be achieved at a critical relative humidity below the ambient relative humidity in the mine (approximately 68%).

In September 2016, 13 months after starting the test (the load was not increased during Stage 2), the strain unexpectedly began increasing. The sample height increased, even though the applied stress was compressive and unchanged, as shown in Fig. 11. All four displacement sensors exhibit similar responses; however, rotation of the upper plate can be deduced from the observations, as explained in Sect. 4.4. This "swelling" effect was puzzling and continued for 6 months.

Six months after the swelling was originally detected, the four displacement sensors measured nearly identical changes (i.e., displacement curves parallel to each other), and the average strain rate correlated with what was observed before the swelling period. A possible explanation for this phenomenon is that hydrating anhydrite (or another grain-boundary mineral) results in the formation of gypsum (or another mineral) with a larger molar volume. Hydration was facilitated by dilation that was generated over a period of time after applying the load, which led to exposure of grain boundaries inside the specimen to mine humidity. Initially, this volume increase expelled the grain-boundary hydrocarbons but later caused minor swelling of the sample until the hydration of the grain-boundary phase was complete. This phenomenon will be investigated in more detail in the future.

6.4 Behavior of the Hauterives Sample

The behavior of the Hauterives sample (HR #1) is easier to interpret than the other samples, because HR #1 exhibits features that are consistent with the fundamental understanding of salt behavior. As shown in Fig. 12, the transient phases are shorter than 8 months, as indicated by the stable strain rates at the end of each stage. Given the strain rates identified at the end of the three stages, a power law with an exponent close to $n = 1$ provides a reasonable fit to the data. Strain rates are slower for the Hauterives sample than those of the four other samples. After 8 months at an applied load of 0.2 MPa, the inferred strain rate is $\dot{\varepsilon} = 3 \times 10^{-13}$/s, which is
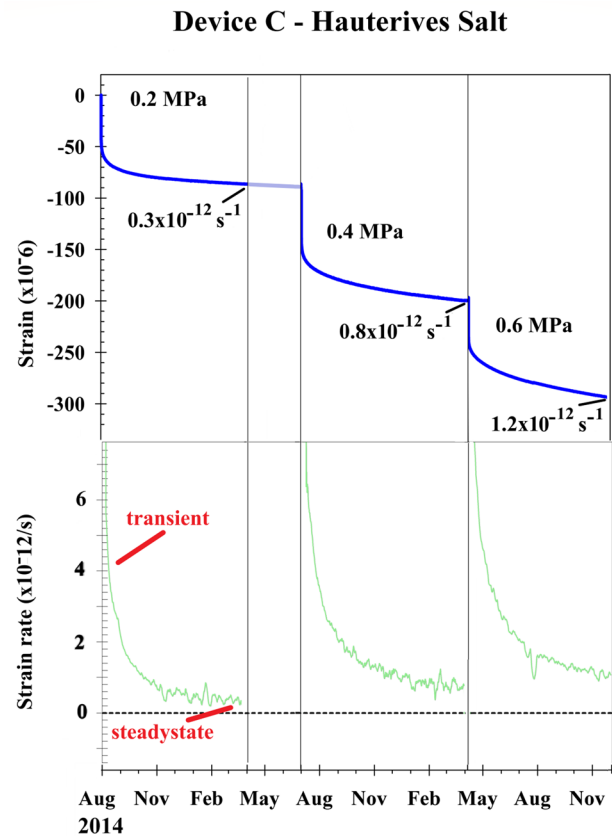

Fig. 12 Strain-versus-time and strain rate-versus-time in the case of the Hauterives sample

the slowest in this series and, to our knowledge, the slowest ever measured during a creep test at a laboratory. This result is somewhat surprising, because the salt of the Valence basin is known to be creep-prone (i.e., the Tersanne gas-storage caverns experienced larger volume losses than other cavern fields). The average amount of insoluble that was determined by an independent study for various Hauterives salt layers includes 8–10% anhydrite and 4–6% clay. The sample used for this test contains a higher than average amount of insoluble (see Sect. 5.1), which may explain why such a slow rate was observed.

6.5 Creep Rates at the End of Each Stage

Strain rates during a 10-day interval at the end of each stage were computed using a least-squares method and are shown in Table 5. Computed strain rates were found to be sensitive to the length of the selected interval fit and the amount of scatter inherent to the data. Uncertainty for the computed strain rates is likely less than 10%. These strain-rate results are shown graphically in Fig. 13. A vertical arrow in Fig. 13 suggests that steady state was not reached at the end of the test stage.

Table 5 Creep rates after each stage

	A (AI #1)	B (AI #2)	C (HR #1)	D (Go #1)	E (Go #2)
Stage 1 (after 11 months)	0.2 MPa 7.5×10^{-12}/s	0.2 MPa 3×10^{-12}/s	0.2 MPa 0.3×10^{-12}/s	0.2 MPa 3×10^{-12}/s	0.2 MPa 2–3×10^{-12}/s
Stage 2 (after 9 months)	0.4 MPa 5.5×10^{-12}/s	0.2 MPa 1.1×10^{-12}/s	0.4 MPa 0.8×10^{-12}/s	0.2 MPa 2.5×10^{-12}/s	0.4 MPa n/a
Stage 3 (after 8 months)	0.6 MPa 6.3×10^{-12}/s	0.6 MPa 4.8×10^{-12}/s	0.6 MPa 1.2×10^{-12}/s	1.07 MPa 12.5×10^{-12}/s	0.6 MPa n/a
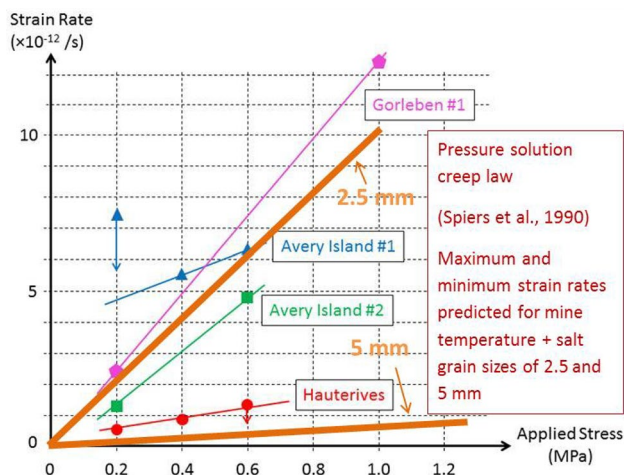
Fig. 13 Strain rates after each test stage as a function of the applied stress. A vertical arrow suggests that steady state had not been reached at the end of the stage. The Gorleben #2 sample is not represented, because swelling was active. The predictions of the pressure-solution creep law of Spiers et al. (1990) are added for rock salt with grain sizes of $D = 2.5$ and 5 mm

6.5.1 Extrapolation of High-Stress Steady-State Strain Results

An important conclusion was derived from the steady-state strain-rate results determined for all five samples: they are much faster than those predicted by extrapolating the high-stress creep test results. For example, several high-stress creep tests have been performed on Avery Island (DeVries 1988) and Gorleben (Bornemann et al. 2008) salts. Power laws have been fit to the reported steady-state rates that were observed during these tests using a stress exponent of $n = 5$. When extrapolated to the low-stress conditions of $\sigma = 0.2$ MPa and $T = 281$ K (8 °C), the following steady-state rates are computed: $\dot{\varepsilon}_s = 1.3 \times 10^{-19}$ s^{-1} (Avery Island salt) and $\dot{\varepsilon}_s = 3.1$–$6.2 \times 10^{-20}$ s^{-1} (Gorleben salt). The as-observed steady-state strain rates (Table 5) are 7–8 orders of magnitude faster than the extrapolated strain rates for the Avery Island and Gorleben salts.

6.5.2 Strain-Rate Dependency on Grain Size

Grain sizes for the tested salts ranged from approximately 3.5–11 mm. The coarsest grained salt (Hauterives) was found to produce the slowest strain rates, while the finest grained salt (Gorleben) had the fastest strain rates. The average grain size of the Avery Island salt is between the grain sizes of the other two salts and its rates are between the observed strain rates of the two other salts. These results are consistent with Eq. (6) prediction. Interestingly, the observed steady-state strain rates and equivalent viscosities in the range of 10^{17}–10^{18} Pa s fall within the range expected for pressure-solution creep of rock salt (Spiers et al. 1990) and given by the second term in Eq. (6) with grain sizes (D) of 2.5–5 mm (see Fig. 13). Grain sizes that ranged from 2.5 to 5 mm span the range for Gorleben salt and are within a factor of approximately 2 for the range of grain sizes of the other samples (i.e., $D = 4$, 8, and 10 mm for the Gorleben, Avery Island, and Hauterives samples, respectively). The inverse cubic dependency of grain size on the pressure-solution strain rate (Spiers et al. 1990) is also consistent with strain rates that are approximately 1 order of magnitude faster and observed in the present Gorleben samples ($D = 4$ mm) compared to the Hauterives sample ($D = 10$ mm).

6.5.3 Power on Stress

For creep at low stresses, the test results confirm that the dependency between the deviatoric stress and strain rate is lesser than the dependency at high stresses. The exponent of the power-law exponent seems to be slightly higher than 1 for the Hauterives sample and the Go #1 sample. For the Go #1 sample, the steady-state strain rate increased by a factor of 5 for a load increase from 0.2 to 1.07 MPa.

For the Avery Island samples, comparison is more difficult, because the steady state was not fully reached by AI #1 during each stage of the test (i.e., the strain rate was still decreasing at the end of the first two stages before the additional load was applied). The behavior of samples AI #1 and AI #2 is also slightly different and does not replicate each other, which can be seen in Fig. 14. Although the specimens were taken from a block within centimeters of each other, AI #1 was set in an oil-filled container and AI #2

Fig. 14 Steady-state strain rates for four low-stress creep tests on Avery Island samples. Each number in parentheses is the creep stage duration in months
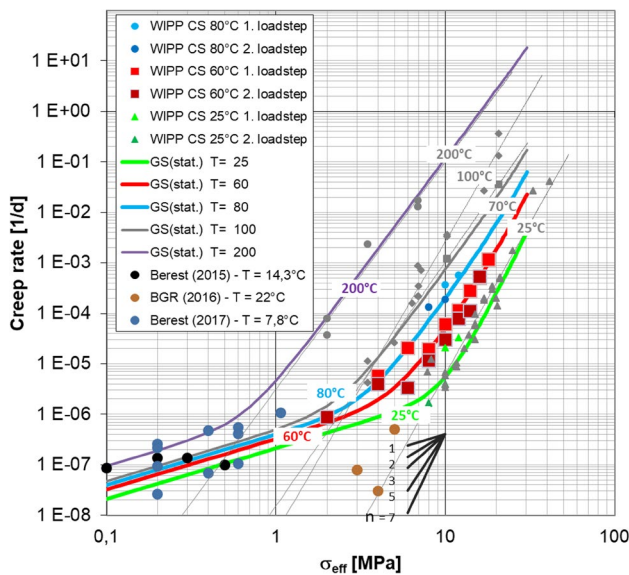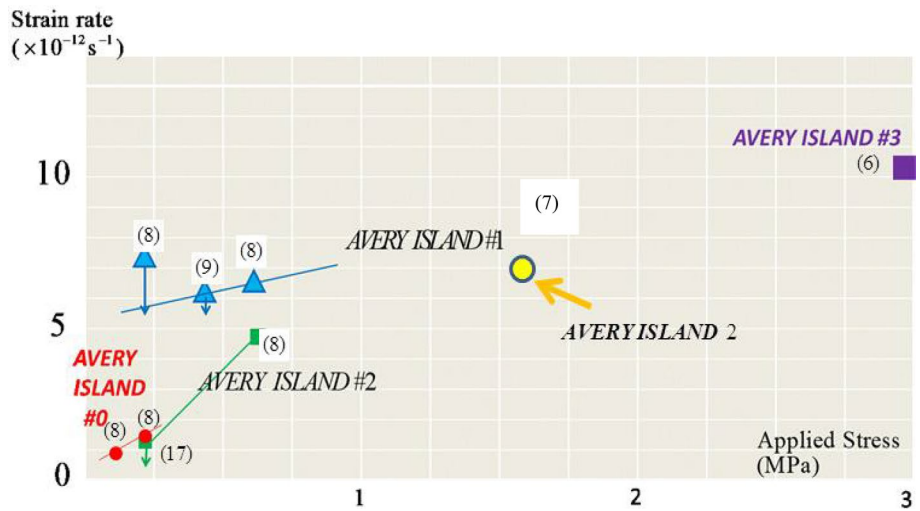

Fig. 15 "Synoptic View of Laboratory Creep Test Results on Waste Isolation Pilot Plant Salt in Relation to Findings From Creep Tests on Various Salt Specimens at Low Deviatoric Stresses. The various datasets are fitted by using the Günther/Salzer-material law", reproduced from Herchen et al. (2018). Each dot corresponds to one creep test. Results suggest a change in the exponent of the power law when deviatoric stresses are low

was exposed to the air. While the effect of this difference is unknown, the results of AI #2 suggest that the power-law exponent is slightly higher than in AI #1 (the steady-state strain rate increased by a factor of 4 for a load increase from 0.2 to 0.6 MPa). If AI #1 did not reach a steady state during the first stage, the results of AI #1 are consistent with this interpretation.

In addition to the data collected from the tests performed at the Altaussee mine, low-stress creep data are

also available from two other tests that were performed on the Avery Island salt (Fig. 14). In addition, a later test, 7-month long, performed on the Avery#2 sample at a load of 1.59 MPa, performed in the frame of the new program mentioned in Sect. 7, was also represented. A similar multistep test (AI #0) was performed in the Varangéville Mine at an ambient temperature of 13.5 °C (Bérest et al. 2014). The test on AI #0 consisted of two 8-month stages at loads of 0.1 and 0.2 MPa, respectively. At the end of the first stage, the strain rate was $\dot{\varepsilon}_s = 0.99 \times 10^{-12}$ s^{-1} compared to the strain rate of $\dot{\varepsilon}_s = 1.59 \times 10^{-12}$ s^{-1} at the end of the second stage. A fourth test was conducted on Avery Island salt in the Altaussee mine in 2017 at a 3 MPa load (the testing device was slightly modified) to fill the gap between the 0–1-MPa stress range and the 5–15-MPa stress range (AI #4). After 6 months, the strain rate of AI #4 had more or less stabilized at $\dot{\varepsilon}_s = 1.1 \times 10^{-11}$ s^{-1}. After completing AI #4 test in the mine, the specimen was retested at the RESPEC laboratory in Rapid City, South Dakota, United States, under essentially the same conditions as those at the mine (8 °C and 3 MPa deviatoric stress). The laboratory test was performed in two parts: (1) 7 weeks at unconfined conditions (oil was in the pressure vessel to allow cooling of the specimen but not pressurized) and (2) 3 weeks with a 5 MPa confining pressure at the same deviatoric stress of 3 MPa. The strain-rate results at the end of both stages were the same $\left(\dot{\varepsilon}_s = 1.8 \times 10^{-11}\ \text{s}^{-1}\right)$ and consistent with what had been measured in the mine. Because the measured strain rates of AI #4 at the mine and in the laboratory under confined and unconfined conditions are essentially the same, steady state was likely reached, and dilation of the specimen at unconfined conditions (if it occurred) does not significantly affect the strain rate at low deviatoric stress.

6.6 Discussion

Equation (6) predicts that the primary mechanisms governing the creep rate of salt are controlled by dislocation (first term) and diffusional (second term) mechanisms. Equation (7) further assumes that diffusional creep is sensitive to grain size and that the strain rate is a linear function of stress (i.e., no exponent on stress). The test results presented here support the conclusion that pressure solution is the dominant deformation mechanism at low-stress and steady-state strain rates can be reasonably approximated using a linear relationship with stress. The results also quantitatively agree that an inverse cubic relationship exists between the grain size and strain rate in the regime of the current experiments. However, the observed creep rates reported in Table 5 are 3–10 times faster than the absolute rates expected from the Spiers et al. (1990) pressure-solution model when applied for the average grain sizes of the specimens tested. While this phenomenon has not been explained, fluid-assisted recrystallization and/or microcracking that causes grain-size reduction in the present tests could partially explain this discrepancy.

6.7 A Tentative Synthesis

The database that was obtained from in situ observations and laboratory tests on salt indicates that dislocation (e.g., Carter and Hansen 1980) and diffusional creep mechanisms (e.g., Urai and Spiers 2007; Spiers et al. 1990) can be important when evaluating the mechanical behavior of salt. The implications of these different creep mechanisms for constitutive model development become apparent in Fig. 15, which shows the experimental data sets for the Waste Isolation Pilot Plant (WIPP) salt in relation with the findings from the present study and earlier tests with different salt types. The stress response on salt creep is characterized by a change in slope from a stress exponent of 3–7 for stresses greater than 5 MPa to a stress exponent of approximately 1 for stresses less than 5 MPa. The WIPP data suggest that the transition stress value is temperature-dependent and decreases as the temperature increases. This observation may confirm the process of water-assisted creep mechanism(s) at low stresses that is believed to be active in salt glaciers or salt formations with increased water content. Although the number of tests is limited, the 2016 tests that were performed by BGR on the Morsleben salt using uniaxial test rigs in the 3–5 MPa range (Herchen et al. 2018) suggest a behavior that is more consistent to a power law with a stress exponent of approximately 5, which is interpreted as the process of dislocation creep.

7 Conclusions

The test results from this study promote the following conclusions:

- For low-stress creep tests, transient creep is longer than generally perceived.
- Steady-state strain rates for low-stress tests are much faster (by 7–8 orders of magnitude) than the rates extrapolated from high-stress tests.
- The exponent of the power law in the low-stress domain appears to be close to $n = 1$ (instead of $n = 5$ in the high-stress domain in the case of the Gorleben and Avery Island salts).

When these conclusions are accepted, salt behaves in the low–stress domain ($\sigma \approx 0.1$–1 MPa) as a Newtonian fluid with a viscosity of $\eta \approx 10^{17}$ Pa s. This value is consistent with values inferred from back-calculations of salt dome rise, which is a phenomenon that implies relatively small deviatoric stresses. Obviously, the possible existence of a threshold for viscoplastic deformation when deviatoric stress is smaller than 0.1 MPa is still an open question. This value is also consistent with the process of pressure-solution creep as the dominant deformation mechanism, which is presented by Spiers et al. (1990). The dominant role of pressure-solution creep is further supported, because the samples described in this study indicate an increase in strain rate with a decrease in grain size.

As mentioned in the introduction, these conclusions have important consequences for the computation of salt mines and salt caverns. They predict that, if the standard power law applies at the vicinity of a cavern, a modified creep law must be adopted in the far field, where deviatoric stresses are non-zero but small. It can be expected that creep closure rate is faster and transient structural response is shorter.

Several questions remain. A blind zone, or region of limited or no experimental evidence, remains in the 1–5 MPa stress regime. The micro-mechanisms that are responsible for salt creep in the $\sigma < 5$ MPa stress domain are not well understood (i.e., the role of hygrometry and brine content remains to be investigated). Only uniaxial tests were performed during this program and the role of a confining pressure requires further investigation. To address these issues, a new testing program that is supported by the SMRI was initiated in the fall of 2017, and the authors recognize the SMRI's consistent efforts to promote scientific research for the benefit of the salt industry.

References

Bérest P (2013) The mechanical behavior of salt and salt caverns. Key note lecture. In: Marek Kwasniewśki M, Lydżba D (eds) Proceedings Eurock 2013. CRC Press, London, pp 17–30

Bérest P, Blum PA, Charpentier JP, Gharbi H, Valès F (2005) Very slow creep tests on rock samples. Int J Rock Mech Min Sci 42:569–576

Bérest P, Brouard B, Karimi-Jafari M (2009) The effect of small deviatoric stresses on cavern creep behavior. In: Zuoliang S (ed) Proceedings 9th international symposium on salt. Gold Wall Press, Beijing, China, pp 574–589

Bérest P, Béraud JF, Gharbi H, Brouard B, DeVries K (2014) A very slow creep test on an Avery Island salt sample. In: Proceedings 48th US rock mechanics/geomechanics symposium, Minneapolis, Minnesota

Bérest P, Brouard B, Gharbi H (2015) Rheological and geometrical reverse creep in salt caverns. In: Roberts LA, Mellegard KD, Hansen F (eds) Mechanical behavior of salt VIII: proceedings of the conference on mechanical behavior of salt, SALTMECH VIII. CRC Press/Balkema, Leiden, The Netherlands, pp 199–208. https://www.crcpress.com/Mechanical-Behaviour-of-Salt-VIII/Roberts-Mellegard-Hansen/p/book/9781138028401

Bérest P, Brouard B, Bruckner D, DeVries K, Gharbi H, Hévin G, Gerd G, Hofer G, Spiers C, Stimmisher S, Urai JL (2017) Very slow creep tests as a basis for cavern stability analysis. SMRI research report RR2017-1, SMRI, Clarks Summit, PA

Blum W, Fleischman C (1988) On the deformation-mechanism map of rock salt. In Hardy R Jr, Langer M (eds) Proceedings of the second conference on the mechanical behavior of salt. H. Trans TechPub. Clausthal-Zellerfeld, Germany, pp 7–23

Bornemann O, Behlau J, Keller S, Mingerzahn G, Schramm M (2008) Standortbeschreibung gorleben teil III: ergebnisse der erkundung des salinars, abschlussbericht zum AP G 412110000. Bundesanstalt für Geowissenschaften und Rohstoffe, Hanover

Breunesse JN, van Eijs RMHE, de Meer S, Kroon JC (2003) Observation and prediction of the relation between salt creep and land subsidence in solution-mining. The Barradeel case. In: Proceedings SMRI fall meeting, Chester, UK, pp 38–57

Brouard B, Bérest P, de Greef V, Béraud JF, Lheur C, Hertz E (2013) Creep closure rate of a shallow salt cavern at Gellenoncourt, France. Int J Rock Mech Min Sci 62:42–50. https://doi.org/10.1016/j.ijrmms.2012.12.030

Campos de Orellana AJ (1996) Non-associated pressure solution creep in salt rock mines. In: Aubertin M, Hardy RH Jr (eds) Proceedings of the fourth conference on the mechanical behavior of salt. Trans Tech Pub, Clausthal-Zellerfel, Germany, pp 429–444

Carter NL, Hansen FD (1980) Mechanical behavior of Avery Island halite: a preliminary analysis. Report Number ONWI100, prepared by RESPEC Inc., Rapid City, SD, for the Office of Nuclear Waste Isolation. Battelle Memorial Institute, Columbus. https://inis.iaea.org/search/search.aspx?orig_q=RN:12577452

Carter NL, Horseman ST, Russell JE, Handin J (1993) Rheology of rocksalt. J Str Geo 15:1257–1271. https://doi.org/10.1016/0191-8141(93)90168-A

Chan KS, Munson DE, Fossum AF, Bodner SR (1996) A constitutive model for representing coupled creep, fracture and healing in rock salt. In: Aubertin M, Hardy, RH Jr (eds) Proceedings of the fourth conference on the mechanical behavior of salt. Trans Tech Pub, Clausthal-Zellerfel, Germany, pp 221–247

Cornet JS, Dabrowski M, Schmid DW (2017) Long-term cavity closure in non-linear rocks. Geo J Int 210:1231–1243

Cristescu ND, Hunsche U (1998) Time effects in rock mechanics. Series: materials, modelling and computation. Wiley, Chichester

DeVries KL (1988) Viscoplastic laws for Avery Island salt. RSI0333, prepared by RE/SPEC Inc., Rapid City. SD, for Stone & Webster Engineering Corporation, Boston

Djizanne Djakeun H (2014) Stabilité mécanique d'une cavité saline soumise à des variations rapides de pression. Dissertation. Ecole Polytechnique, Palaiseau, France

Hammer J, Pusch M, Häger A, Ostertag-Henning C, Thiemeyer N, Zulauf G (2015) Hydrocarbons in rock salt of the Gorleben salt dome—amount, distribution, origin, and influence on geomechanical properties. In: Roberts LA, Mellegard KD, Hansen F (eds) Mechanical behavior of salt VIII: proceedings of the conference on mechanical behavior of salt, SALTMECH VIII. CRC Press/Balkema, Leiden, The Netherlands, pp 69–75. https://www.crcpress.com/Mechanical-Behaviour-of-Salt-VIII/Roberts-Mellegard-Hansen/p/book/9781138028401

Hampel A (2015) Description of damage reduction and healing with the CDM constitutive model. In: Roberts LA, Mellegard, KD, Hansen F (eds) Mechanical behavior of salt VIII: proceedings of the conference on mechanical behavior of salt, SALTMECH VIII. CRC Press/Balkema, Leiden, The Netherlands, pp 301–310. https://www.crcpress.com/Mechanical-Behaviour-of-Salt-VIII/Roberts-Mellegard-Hansen/p/book/9781138028401

Herchen K, Popp T, Düsterloh U, Lux KH, Salzer K, Lüdeling C, Günther RM, Rölke C, Minkley W, Hampel A, Yildirim S, Staudtmeister K, Gährken A, Stahlmann J, Reedlunn B, Hansen FD (2018) WEIMOS: laboratory investigations of damage reduction and creep at small deviatoric stresses in rock salt. In: Proceedings of the conference on mechanical behavior of salt, SaltMech IX, Hannover, Germany, September 12–18, pp 175–192

Horseman ST (1988) Moisture content—a major uncertainty in storage cavity closure prediction. In: Hardy HR Jr, Langer M (eds) Proceedings of the second conference on the mechanical behavior of salt. Trans Tech Publications, Clausthal, Germany, pp 53–68

Hunsche U (1988) Measurement of creep in rock salt at small strain rates. In: Hardy HR Jr, Langer M (eds) Proceedings of the second conference on the mechanical behavior of salt. Trans Tech Publications, Clausthal, Germany, pp 187–196

Hunsche U, Schultze O (1996) Effect of humidity and confining pressure on creep of rock salt. In: Hardy HR Jr, Langer M (eds) Proceedings of the third conference on the mechanical behavior of salt. Trans Tech Publications, Clausthal, Germany, pp 237–248

Hunsche U, Schultze O (2002) Humidity induced creep and its relation to the dilatancy boundary. In: Cristescu ND, Hardy JR Jr, Simionescu RO (eds) Proceedings of the fifth conference on the mechanical behavior of salt. A. A. Balkema, The Netherlands, pp 73–87

Koelemeijer PJ, Peach CJ, Spiers CJ (2012) Surface diffusivity of cleaved NaCl crystals as a function of humidity: impedance spectroscopy measurements and implications for crack healing in rock salt. J Geo Res Solid Earth 117:1–15. https://doi.org/10.1029/2011JB008627

Langer M (1984) The rheological behavior of rock salt. In: Hardy HR Jr, Langer M (eds) Proceedings of the second conference on the mechanical behavior of salt. Trans Tech Publications, Clausthal, Germany, pp 201–240

Lux KH, Düsterloh U (2015) From birth to long-term life—main aspects regarding THM-coupled simulation of salt cavern behavior as well as regarding improved salt cavern design with special consideration of rock salt damage. In: Roberts LA,

Mellegard KD, Hansen F (eds) Mechanical behavior of salt VIII: proceedings of the conference on mechanical behavior of salt, SALTMECH VIII. CRC Press/Balkema, Leiden, The Netherlands, pp 273–280

Marketos G, Spiers CJ, Govers R (2016) Impact of rock salt creep law choice on subsidence calculations for hydrocarbon reservoirs overlain by evaporite caprocks. J Geo Res Solid Earth 121:4249–4267. https://dspace.library.uu.nl/handle/1874/335958

Munson DE (1979) Preliminary deformation-mechanism map for salt (with application to WIPP), SAND79-0076 report. Sandia National Laboratories, Albuquerque

Munson DE, Dawson PR (1984) Salt constitutive modeling using mechanism maps. In: Hardy HR Jr, Langer M (eds) Proceedings of the first conference on the mechanical behavior of salt. Trans TechPu. Clausthal-Zellerfeld, Germany, pp 717–737

Peach CJ, Spiers CJ, Trimby PW (2001) Effect of confining pressure on dilatation, recrystallization, and flow of rock salt at 150 °C. J Geo Res Solid Earth 106:13315–13328. https://doi.org/10.1029/2000JB900300

Perrier F, Le Mouël JL, Richon P (2010) Spatial and temporal dependence of temperature variations induced by atmospheric pressure variations in shallow underground cavities. Pure Appl Geophys 167: 253–276. https://doi.org/10.1007/s00024-009-0016-1

Popp T, Kern H, Schultze O (2002) Permeation and development of dilatancy in rock salt. In: Cristescu ND, Hardy HR Jr, Simionescu RO (eds) Proceedings of the fifth conference the mechanical behavior of salt. Swets & Zeitlinger, Lisse, pp 95–124

Popp T, Minkley W, Salzer K, Schulze O (2012) Gas transport properties of rock salt—synoptic view. In: Bérest P, Ghoreychi M, Hadj-Hassen F, Tijani M (eds) Proceedings of the seventh conference on the mechanical behavior of salt. Taylor & Francis Group, London, UK, pp 143–153

Rokahr R, Staudtmeister K, Zapf D (2011) Rock mechanical design for a planned gas cavern field in the Preesall project area, Lancashire, UK. In: Proceedings SMRI fall meeting, York, UK, pp 189–203

Schultze O (2007) Investigations on damage and healing in rocks. In: Wallner M, Lux KH, Minkley W, Hardy RH Jr (eds) Proceedings of the sixth conference the mechanical behavior of salt. Taylor & Francis, London, UK, pp 33–44

Spiers CJ, Schutjens PMTM, Brzesowsky RH, Peach CJ, Liezenberg JL, Zwart HJ (1990) Experimental determination of the constitutive parameters governing creep of rocksalt by pressure solution. Geological society special publication 54, Deformation mechanisms, rheology and tectonics, The Geological Society, London, England, vol 54, pp 215–227. https://doi.org/10.1144/GSL.SP.1990.054.01.21

Ter Heege JH, De Bresser JHP, Spiers CJ (2005a) Rheological behaviour of synthetic rocksalt: the interplay between water, dynamic recrystallization and deformation mechanisms. J Struct Geo 27:948–963. https://doi.org/10.1016/j.jsg.2005.04.008

Ter Heege JH, De Bresser JHP, Spiers CJ (2005b) Dynamic recrystallization of wet synthetic polycrystalline halite: dependence of grain size distribution on flow stress, temperature and strain. Tectonophysics 396:35–57. https://doi.org/10.1016/j.tecto.2004.10.002

Thorel L, Ghoreychi M (1993) Rock salt damage. Experimental results and interpretation. In: Hardy HR Jr, Langer M (eds) Proceedings of the third conference on the mechanical behavior of salt. Trans Tech Publications, Clausthal, Germany, pp 175–189

Urai JL, Spiers CJ (2007) The effect of grain boundary water on deformation mechanisms and rheology of rocksalt during long-term deformation. In: Wallner M, Lux K, Minkley W, Hardy H Jr (eds) Proceedings of the sixth conference on the mechanical behavior of salt. A. A. Balkema, The Netherlands, pp 149–158

Urai JL, Schléder Z, Spiers CJ, Kukla PA, Lange JM, Röhling HG (2008) Flow and transport properties of salt rocks. In: Littke R, Bayer U, Gajewski D, Nelskamp S (eds) Dynamics of complex intracontinental basins: the central European basin system. Springer, Berlin, pp 277–290

Van Sambeek LL (2012) Measurements of humidity-enhanced salt creep in salt mines: proving the Joffé effect. In: Bérest P, Ghoreychi M, Hadj-Hassen F, Tijani M (eds) Proceedings of the 7th conference on the mechanical behavior of salt. Taylor & Francis Group, London, UK, pp 179–184

Van Sambeek LL, DiRienzo AL (2016) Analytical solutions for stress distributions and creep closure around open holes or caverns using multilinear segmented creep laws. In: Proceedings SMRI fall meeting, Salzburg, Austria, September 26–28, pp 225–238

Van Sambeek L, Fossum A, Callahan G, Ratigan J (1993) Salt Mechanics: Empirical and Theoretical Developments. In: Hidekate Kakihana, Hardy RH Jr, Hoshi T, Toyokura K (eds) Proceedings seventh symposium on salt, vol I. Elsevier, Amsterdam, The Netherlands, pp 127–134

Wawersik WR, Preece DS (1984) Creep testing of salt—procedures, problems and suggestions. In: Hardy HR Jr, Langer M (eds) Proceedings of the first conference on the mechanical behavior of salt. Trans Tech Publications, Clausthal, Germany, pp 421–449